Supporting Information on "Revealing Transient Shuttling Mechanism of Catalytic Ion Transport through Liquid-Liquid Interface"

Ai Koizumi,[†] Hirofumi Tahara,[†] Tomonori Hirano,[†] and Akihiro Morita[*,†,‡]

Department of Chemistry, Graduate School of Science, Tohoku University Aoba-ku, Sendai 980-8578, Japan , and Elements Strategy Initiative for Catalysts and Batteries (ESICB), Kyoto University, Kyoto 615-8520, Japan

E-mail: morita@tohoku.ac.jp

The Supporting Information describes the technical details of molecular dynamics (MD) calculations and associated results of calculations.

Contents

[*]To whom correspondence should be addressed
[†]Tohoku University
[‡]Kyoto University

S1 MD Conditions

The present MD simulation investigated the transport of F^- through water-dichloromethane (DCM) interface. The ligand to support ion transport is either tetrahexylammonium ($N(C_6H_{13})_4^+$, THA^+) or tetrabutylammonium ($N(C_4H_9)_4^+$, TBA^+). The MD simulation was carried out with our in-house code, namely FreeFlex.

S1.1 Force fields

The force field parameters of constituent molecules/ions employed in the present MD simulation are summarized in Tables S1 and S2. Water is described with the POL3 model,[1] while DCM with the one developed by Dang et al.[2] F^- is treated with the one by Dang et al.[3] These models have rigid intramolecular geometry and polarizability parameters α at their sites, as the polarizable models are preferred to reproduce the transfer free energies of the ions.[4] We note that the original paper of the DCM model[2] includes some errors in parameters,[5] and the corrected parameters are listed in Table S1.

Table S1: Force field parameters for water, DCM, and F^-.

(a) sites

molecule	site	q (e)	α (Å^3)	σ (Å)	ε (kcal/mol)
water	H	0.3650	0.170	0.000	0.000
	O	-0.7300	0.528	3.204	0.156
DCM	C	-0.2720	0.878	3.410	0.137
	H	0.1897*	0.135	2.400	0.040
	Cl	-0.0537*	1.910	3.450	0.280
F^-	F	-1.0000	1.050	3.3587	0.100

(b) bonds

molecule	bond	length (Å)
water	H-O	1.0
	H-H	1.63328
DCM	C-H	1.070
	C-Cl	1.772
	H-Cl	2.33057
	Cl-Cl	2.92420

* corrected from Ref. [2]. [5]

The force fields of THA^+ and TBA^+ were described on the basis of the united atom model of AMBER ff03ua. [6] The potential functions of internal stretching, bending, and torsional vibrations are given in the following forms, [7,8]

$$V_{\text{bonds}} = \sum_i^{\text{bonds}} k_r^{(i)} \left(r^{(i)} - r_0^{(i)} \right)^2, \tag{S1}$$

$$V_{\text{angles}} = \sum_i^{\text{angles}} k_\theta^{(i)} \left(\theta^{(i)} - \theta_0^{(i)} \right)^2, \tag{S2}$$

$$V_{\text{dihederals}} = \sum_i^{\text{dihedrals}} \Big[V_1^{(i)} \{1 + \cos(\phi^{(i)} - \gamma_1^{(i)})\} + V_2^{(i)} \{1 + \cos(-2\phi^{(i)} - \gamma_2^{(i)})\} + V_3 \{1 + \cos(-3\phi^{(i)} - \gamma_3^{(i)})\} + \frac{1}{2} V_{\text{LJ}} \Big], \tag{S3}$$

$$V_{\text{LJ}} = 4\varepsilon \left[\left(\frac{\sigma}{r} \right)^{12} - \left(\frac{\sigma}{r} \right)^{6} \right] \tag{S4}$$

Note that the dihedral potential in Eq. (S3) includes half the nonbonding 1-4 interaction. The models of THA^+ and TBA^+ include internal flexibility to take account of conformations

of alkyl chains. The force field parameters in Eqs. (S1)-(S4) for THA^+ and TBA^+ are summarized in Table S2, with the site labels shown in Figure S1. The parameters for dihedral angles were slightly modified so as to facilitate conformational change of alkyl chains during the equilibration and sampling.

Table S2: Force field parameters for THA^+ and TBA^+.

(a) sites

site	q (e)	α (Å^3)	σ (Å)	ε (kcal/mol)
N	0.0	0.0	3.250	0.170
C2(a)	0.25	0.0	3.905	0.118
C2(b)	0.0	0.0	3.905	0.118
C3	0.0	0.0	3.905	0.175

(b) bonds

bond	k_r (kcal/mol $\cdot$ Å^2)	r_0 (Å)
N-C2	367.0	1.471
C2-C2	310.0	1.526
C2-C3	310.0	1.526

(c) angles

bond	k_θ (kcal/mol $\cdot$ degree^2)	θ_0 (degree)
C2-N-C2	50.0	109.50
N-C2-C2	80.0	111.20
C2-C2-C2	40.0	109.50
C2-C2-C3	40.0	109.50

(d) dihedral angles

bond	V_n (kcal/mol $\cdot$ degree^2)	γ_n (degree)
N-C2-C2-C2	1.00	180.0
	0.24	180.0
	1.12	0.0
C2-C2-C2-C2	1.00	180.0
	0.24	180.0
	1.12	0.0
C2-C2-C2-C3	1.00	180.0
	0.24	180.0
	1.12	0.0

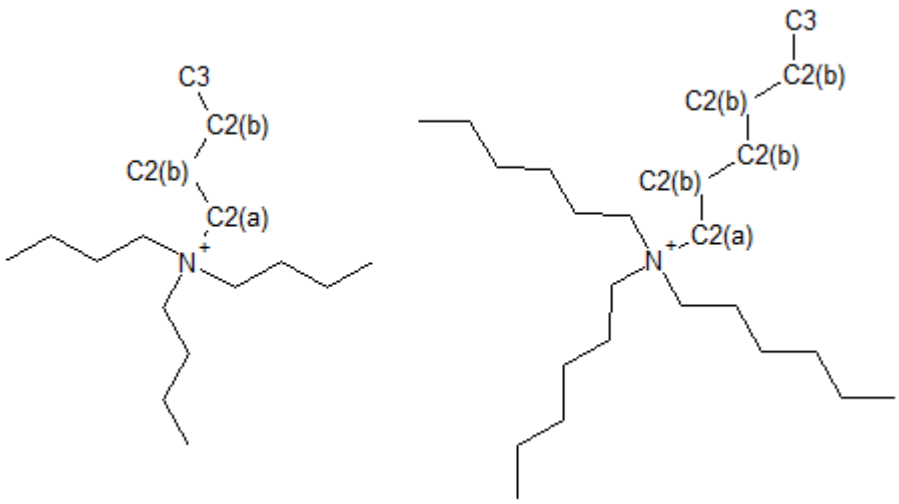

Figure S1: Schematic of TBA^+ (left) and THA^+ (right) molecules with the site labels.

S1.2 MD cells

The present work adopted four different dimensions of MD cells (A)-(D) for different purposes. The cell (A) was mainly used for the free energy calculations of the water-DCM system, and is illustrated in Figure S2. The dimensions of the cell (A) are $L_x \times L_y \times L_z = 50$ Å $\times 50$ Å $\times 115$ Å with the 3-dimensional periodic boundary conditions. The cell contains one anion (F^-), one counter ion (THA^+ or TBA^+), 2091 water, and 2116 DCM molecules. The water and DCM phases form alternating slabs with interfaces normal to the z axis. The thicknesses of water and DCM phases are about 25 Å and 90 Å, respectively, along the z axis. We also imposed electric field $E_z = 0.0$, 0.1, 0.2 V/nm along the z axis to mimic experimental electrochemical conditions. Accordingly, a site of partial charge q feels extra force $-qE_z$ from the field during the MD simulation.

The other three smaller cells (B)-(D) were employed for auxiliary MD calculations. (B) The transfer of single anion (F^-) or cation (THA^+ or TBA^+) was treated using an MD cell of $L_x \times L_y \times L_z = 25$ Å $\times 25$ Å $\times 85$ Å with the 3-dimensional periodic boundary conditions. The cell contains one ion (either anion or cation), 523 water and 353 DCM molecules, and the water and DCM form alternating slabs with thicknesses of 25 Å and 60 Å, respectively. (C) Solvation structures of water around the ions were investigated in an

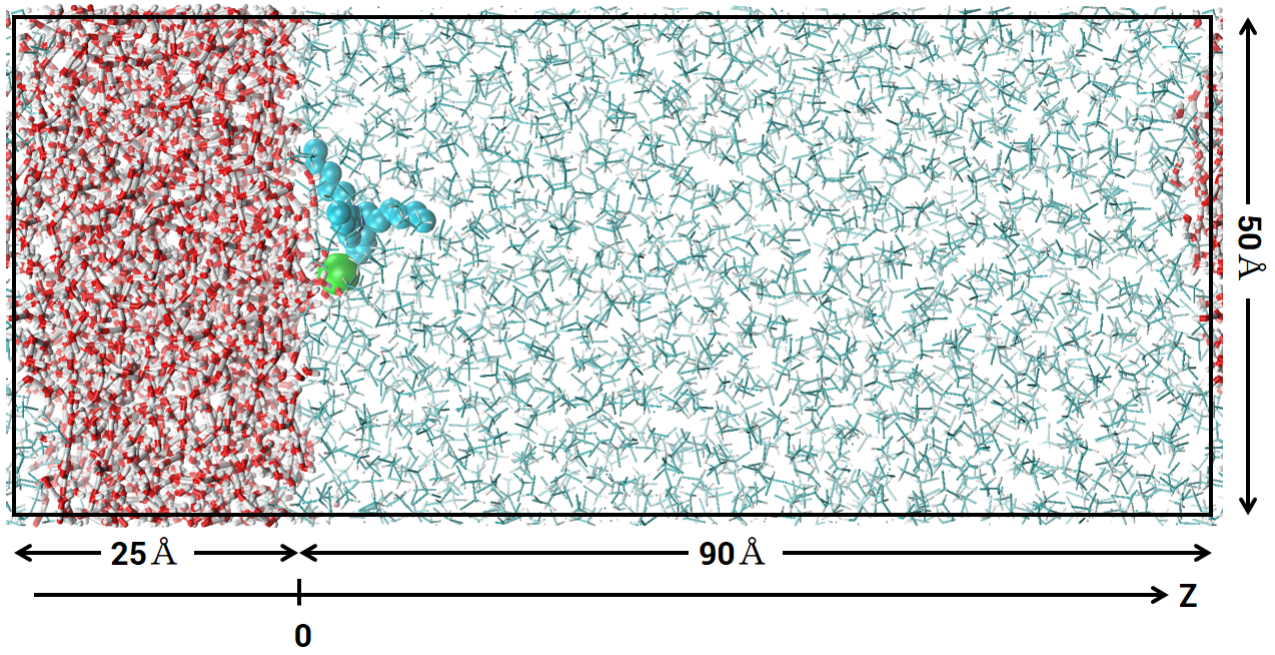

Figure S2: Geometry of MD cell (A) for $G^{(2)}(z, r)$ calculations.

MD cell of $L_x \times L_y \times L_z = 25$ Å $\times$ 25 Å $\times$ 25 Å with the 3-dimensional periodic boundary conditions. The cell contains one ion and 523 water molecules. (D) Dissociation between ion and counter ion was investigated in an MD cell of $L_x \times L_y \times L_z = 25$ Å $\times$ 25 Å $\times$ 50 Å with the 3-dimensional periodic boundary conditions. The cell contains one anion, one cation (THA^+ or TBA^+) and 294 DCM molecules.

In all cases of cells (A)-(D), the long-range electrostatic interactions were treated with the Particle-Mesh Ewald (PME) method.[9] The Ewald separation parameter κ is set to 0.323 $Å^{-1}$. The dipolar interaction in the PME was treated by the smooth PME (SPME) method of Toukmaji *et al.*[10] The 6-th order Cardinal B-splines were employed for the interpolation with grid spacing about 0.7 Å.

S1.3 Coordinates for free energy surfaces

The two-dimensional free energy surface $G^{(2)}(z, r)$ associated to the ion transfer with complex formation is represented by two coordinates, z and r. z is the normal coordinate of the

anion (F^-) from the liquid-liquid interface, where $z = 0$ is set at the Gibbs dividing surface of water, and $z < 0$ ($z > 0$) indicates the anion in the water (oil) phase. We defined the z coordinate with respect to the Gibbs dividing surface rather than the intrinsic surface,[11] and the structural fluctuation of interface associated to the ion transfer was accounted for with the water finger coordinate w as discussed below. The second coordinate r denotes the distance between anion and ligand (THA^+/TBA^+). In the present work, r is defined with the distance between the anion (F^-) and the central nitrogen (N) site of THA^+/TBA^+.

The two-dimensional surface $G^{(2)}(z, r)$ was obtained by replica exchange umbrella sampling (REUS).[12] In the (z, r) surface, bias potentials of the following form were employed,

$$U^{\text{bias}}(z, r;\ z_0, \sigma_z, r_0, \sigma_r) = \frac{k_B T}{2} \left\{ \frac{(z - z_0)^2}{\sigma_z^2} + \frac{(r - r_0)}{\sigma_r^2} \right\} \tag{S5}$$

where (z_0, r_0) is the center of the umbrella potential, and σ_z and σ_r denote the widths along the z and r directions, respectively. We prepared 480 sets of umbrella potentials with different (z_0, r_0) values as shown in Table S3, and performed parallel MD simulations with different bias potentials. In the stage of equilibration, we set $\sigma_z = 0.5$ Å and $\sigma_r = 0.25$ Å, and then in the sampling stage $\sigma_z = 1.0$ Å and $\sigma_r = 0.5$ Å. During the sampling stage, the exchange of umbrella potentials was carried out by the Metropolis criteria. The exchange of umbrella potential was tried every 1000 MD steps among a pair of potentials that differ by one column and/or row in Table S3. The set of trajectories were analyzed by using the Weighted Histogram Analysis Method (WHAM)[13] to derive the free energy surface.

We also calculated the one-dimensional free energy $G^{(1)}(z)$ for a single anion or cation through the liquid-liquid interface. The z coordinate of the cation is defined with the position of the nitrogen (N) site. The MD calculation of $G^{(1)}(z)$ surface may suffer from the hysteresis problem associated to water finger.[4] The problem arises from the fact that both connected and disconnected structures of water finger at a certain z are hard to be properly sampled due to rare structural transition of water finger during MD simulation. To overcome this sampling

problem, we first calculated two-dimensional free energy surface $G^{(2)}(z, w)$ as a function of z and the water finger coordinate w,[4,14] and then integrated over the w coordinate to obtain $G^{(1)}(z)$ by

$$G^{(1)}(z) = -k_B T \ln \int dw \exp\left(-\frac{G^{(2)}(z, w)}{k_B T}\right) \tag{S6}$$

The calculation of two-dimensional free energy $G^{(2)}(z, w)$ ensures proper sampling of both connected and disconnected water finger structures. The $G^{(2)}(z, w)$ was also calculated with the REUS method after our previous work.[4,14] The umbrella potentials are either two-dimensional,

$$U^{\mathrm{bias,2D}}(z, w;\ z_0, \sigma_z, w_0, \sigma_w) = \frac{k_B T}{2}\left\{\frac{(z - z_0)^2}{\sigma_z^2} + \frac{(w - w_0)}{\sigma_w^2}\right\} \tag{S7}$$

or one-dimensional,

$$U^{\mathrm{bias,1D}}(z;\ z_0, \sigma_z) = \frac{k_B T}{2}\frac{(z - z_0)^2}{\sigma_z^2}. \tag{S8}$$

Table S4 shows the parameters z_0 and w_0 in Eqs. (S7) and (S8). In these potentials, σ_z and σ_w were set to 0.25 Å for the equilibration, and $\sigma_z = \sigma_w = 0.5$ Å for the sampling. The scheme of the replica exchange is same as that in our previous work.[4,14]

The one-dimensional free energy $G^{(1)}(r)$ as a function of the cation-anion distance r in the DCM phase was evaluated to discuss the association and dissociation of the ion pair. The calculation was performed with the REUS method with different umbrella potentials defined in the r coordinate. The umbrella potentials for the purpose are in the following form,

$$U^{\mathrm{bias,1D}}(r;\ r_0, \sigma_r) = \frac{k_B T}{2}\frac{(r - r_0)^2}{\sigma_r^2}. \tag{S9}$$

The parameters r_0 in Eq. (S9) are summarized in Table S5. σ_r was determined in the same manner as in Eq. (S5).

Table S3: Table of umbrella potentials with different (z_0, r_0) values in Eq. (S5). A total of 480 different potentials are numbered from 1 to 480. The colored cells illustrate the pair of replica exchange; the counterparts of a red cell are colored in yellow.

																									r_0 (Å)
	457	458	459	460	461	462	463	464	465	466	467	468	469	470	471	472	473	474	475	476	477	478	479	480	23.0
	433	434	435	436	437	438	439	440	441	442	443	444	445	446	447	448	449	450	451	452	453	454	455	456	22.0
	409	410	411	412	413	414	415	416	417	418	419	420	421	422	423	424	425	426	427	428	429	430	431	432	21.0
	385	386	387	388	389	390	391	392	393	394	395	396	397	398	399	400	401	402	403	404	405	406	407	408	20.0
	361	362	363	364	365	366	367	368	369	370	371	372	373	374	375	376	377	378	379	380	381	382	383	384	19.0
	337	338	339	340	341	342	343	344	345	346	347	348	349	350	351	352	353	354	355	356	357	358	359	360	18.0
	313	314	315	316	317	318	319	320	321	322	323	324	325	326	327	328	329	330	331	332	333	334	335	336	17.0
	289	290	291	292	293	294	295	296	297	298	299	300	301	302	303	304	305	306	307	308	309	310	311	312	16.0
	265	266	267	268	269	270	271	272	273	274	275	276	277	278	279	280	281	282	283	284	285	286	287	288	15.0
	241	242	243	244	245	246	247	248	249	250	251	252	253	254	255	256	257	258	259	260	261	262	263	264	14.0
	217	218	219	220	221	222	223	224	225	226	227	228	229	230	231	232	233	234	235	236	237	238	239	240	13.0
	193	194	195	196	197	198	199	200	201	202	203	204	205	206	207	208	209	210	211	212	213	214	215	216	12.0
	169	170	171	172	173	174	175	176	177	178	179	180	181	182	183	184	185	186	187	188	189	190	191	192	11.0
	145	146	147	148	149	150	151	152	153	154	155	156	157	158	159	160	161	162	163	164	165	166	167	168	10.0
	121	122	123	124	125	126	127	128	129	130	131	132	133	134	135	136	137	138	139	140	141	142	143	144	9.0
	97	98	99	100	101	102	103	104	105	106	107	108	109	110	111	112	113	114	115	116	117	118	119	120	8.0
	73	74	75	76	77	78	79	80	81	82	83	84	85	86	87	88	89	90	91	92	93	94	95	96	7.0
	49	50	51	52	53	54	55	56	57	58	59	60	61	62	63	64	65	66	67	68	69	70	71	72	6.0
	25	26	27	28	29	30	31	32	33	34	35	36	37	38	39	40	41	42	43	44	45	46	47	48	5.0
	1	2	3	4	5	6	7	8	9	10	11	12	13	14	15	16	17	18	19	20	21	22	23	24	4.0
z_0 (Å)	-6.0	-4.0	-2.0	0.0	2.0	4.0	6.0	8.0	10.0	12.0	14.0	16.0	18.0	20.0	22.0	24.0	26.0	28.0	30.0	32.0	34.0	36.0	38.0	40.0	

Table S4: Table of 160 umbrella potentials with different (z_0, w_0) values in Eq. (S7) or z_0 values in Eq. (S8). The umbrella potentials numbered $1 \sim 24$ labelled with $w_0 =$ free indicate the one-dimensional potential of Eq. (S8), while $25 \sim 160$ indicate the two-dimensional potential of Eq. (S7). The colored cells illustrate the pair of replica exchange; the counterparts of a red cell are colored in yellow.

																								w_0 (Å)
																							160	18.0
																						158	159	17.0
																					155	156	157	16.0
																				151	152	153	154	15.0
																			146	147	148	149	150	14.0
																		140	141	142	143	144	145	13.0
																	133	134	135	136	137	138	139	12.0
																125	126	127	128	129	130	131	132	11.0
															116	117	118	119	120	121	122	123	124	10.0
														106	107	108	109	110	111	112	113	114	115	9.0
													95	96	97	98	99	100	101	102	103	104	105	8.0
												83	84	85	86	87	88	89	90	91	92	93	94	7.0
											70	71	72	73	74	75	76	77	78	79	80	81	82	6.0
										56	57	58	59	60	61	62	63	64	65	66	67	68	69	5.0
									41	42	43	44	45	46	47	48	49	50	51	52	53	54	55	4.0
								25	26	27	28	29	30	31	32	33	34	35	36	37	38	39	40	3.0
	1	2	3	4	5	6	7	8	9	10	11	12	13	14	15	16	17	18	19	20	21	22	23	24	free
z_0 (Å)	-2.5	-1.5	-0.5	0.5	1.5	2.5	3.5	4.5	5.5	6.5	7.5	8.5	9.5	10.5	11.5	12.5	13.5	14.5	15.5	16.5	17.5	18.5	19.5	20.5	

Table S5: Table of 20 umbrella potentials with different (r_0) values in Eq. (S9).

	1	2	3	4	5	6	7	8	9	10	11	12	13	14	15	16
r_0 (Å)	4.0	5.0	6.0	7.0	8.0	9.0	10.0	11.0	12.0	13.0	14.0	15.0	16.0	17.0	18.0	19.0

S1.4 MD procedures

We describe the procedures to prepare initial configurations, equilibration, and sampling of MD simulation. In either case MD calculations were performed with NVT ensemble with the temperature T set to 300 K by using Nosé-Hoover thermostat.[15,16] The time development was carried out with the velocity Verlet algorithm with a time step of 1 fs, with the RATTLE constraint algorithm.[17–19]

S1.4.1 $G^{(2)}(z,r)$ for ion pair

The calculations of $G^{(2)}(z,r)$ including an anion (F^-) and a counter ion (THA^+/TBA^+) were carried out with the large MD cell (A) (Figure S2) in Sec. S1.2. Initial configurations of MD simulation were prepared by randomly putting 2091 water molecules in the region of -25 Å $< z < 0$ Å of the MD cell and 2116 DCM molecules in 0 Å $< z <$ 90 Å. We also initially put one anion (F^-) at $(x, y, z) = (0$ Å$, 0$ Å$, -5$ Å) and the N site of THA^+ or TBA^+ at $(x, y, z) = (0$ Å$, 0$ Å$, 15$ Å). Then the steepest descent relaxation was adopted to remove unphysical molecular overlap, and subsequently MD equilibration was carried out for 100 ps.

Then we carried out parallel simulation using parallel computers of 480 nodes. We impose 480 different bias potential functions of Table S3 on these respective replicas, and further equilibrate these replicas with different bias potentials for 100 ps independently in parallel. During the equilibration, the electric field E_z along the z axis is incremented every 10 ps by 1/10 of the target value E_z ($= 0 \sim 0.2$ V/nm). After the parallel equilibration is finished as such, the production run was carried out for 200 ps with the replica exchange umbrella sampling (REUS). The resultant set of MD trajectories were treated with the weighted histogram analysis method (WHAM) to calculate $G^{(2)}(z,r)$. The derivation of the free energy $G^{(2)}(z,r)$ from the probability distributions takes account of the volume element of the z and r coordinates.

S1.4.2 Radial distribution functions

Next, radial distribution functions (RDFs) between the solute ions and water molecules in bulk water were calculated to estimate the contact distances of the solute and water molecules. They are needed for applying the water finger coordinate w to the present systems in Sec. S1.4.3 to judge the connectivity based on the water-water and solute-water distances.[4] We initially put one F^-, THA^+ or TBA^+ ion and 523 water molecules randomly in the MD cell (C) in Sec. S1.2. The steepest descent relaxation was adopted to remove unphysical molecular overlap, and subsequently MD equilibration was carried out for 100 ps. Then the sampling calculations of RDFs were performed for 300 ps for each solute ion.

S1.4.3 Free energy profile for single ion

The free energy profile $G^{(1)}(z)$ of a single anion (F^-) or cation (THA^+/TBA^+) over the water-DCM interface was obtained. Since $G^{(1)}(z)$ is derived from $G^{(2)}(z,w)$ by Eq. (S6), $G^{(2)}(z,w)$ for the single anion or cation was calculated using the MD cell (B) in Sec. S1.2. We randomly put 523 water molecules in -25 Å $< z <$ 0 Å, 353 DCM molecules in 0 Å $< z <$ 60 Å, and one ion at $(x,y,z) = (0\text{ Å}, 0\text{ Å}, 5\text{ Å})$. (The position of THA^+/TBA^+ means that of the N site.) The steepest descent relaxation and subsequent MD equilibration for 100 ps were carried out in the same manner as in Sec. S1.4.1. Then we prepared a total of 160 replicas with different umbrella potentials of Eqs. (S7) or (S8), which are summarized in Table S4. These replicas were equilibrated in parallel for 100 ps using parallel computers of 160 nodes, each of which has different umbrella potential, with gradually imposing the electric field E_z from $E_z = 0$ to the target value. After the equilibration was completed, the REUS calculations were performed for 200 ps for each node in the same manner as in our previous works,[4,14] and the results were analyzed by WHAM to obtain $G^{(2)}(z,w)$. The calculated $G^{(2)}(z,w)$ was reduced to $G^{(1)}(z)$ by Eq. (S6).

S1.4.4 Dissociation of ion pair in oil phase

The free energy profile of $G^{(1)}(r)$ as a function of the distance r between anion (F^-) and cation (THA^+/TBA^+) in the bulk DCM phase was calculated using the REUS sampling along the r coordinate. We initially put one F^- anion at $(x, y, z) = (0\ \text{Å}, 0\ \text{Å}, 15\ \text{Å})$, the N site of THA^+ or TBA^+ at $(x, y, z) = (0\ \text{Å}, 0\ \text{Å}, 5\ \text{Å})$, and 294 DCM molecules randomly in the cell (B) in Sec. S1.2, and the steepest descent relaxation was adopted. Then we prepared 20 umbrella potentials of Eq. (S9) in Table S5. The MD equilibrations with 20 different potentials were carried out for 100 ps independently using parallel computers of 20 nodes. During the equilibration the electric field E_z is gradually imposed from $E_z = 0$ to the target value. The REUS calculations were performed for 1 ns, and the results were analyzed by WHAM to obtain $G^{(1)}(r)$. The derivation of $G^{(1)}(r)$ from the probability distributions takes account of the volume element of the r coordinate.

S2 Supporting Results

S2.1 $G^{(2)}(z, r)$ for F^--THA^+/TBA^+

Here we display the whole calculated free energy surfaces $G^{(2)}(z, r)$ for the F^--THA^+/TBA^+ at $E_z = 0.0$, 0.1, 0.2 V/nm in Figures S3 and S4. Note that Figures S3 (a) and (c) are same as Figure 2 (a) and (b) of the main text, and Figures S4 (a) and (c) are same as Figure 3 (a) and (b) of the main text.

S2.2 Transport of ion pair

We discuss the interfacial transport of ion pairs, $F^- - THA^+$ and $F^- - TBA^+$. To estimate the free energy profiles for the ion pairs, we tentatively restrict the (z, r) surface to $r < 10$

(a)

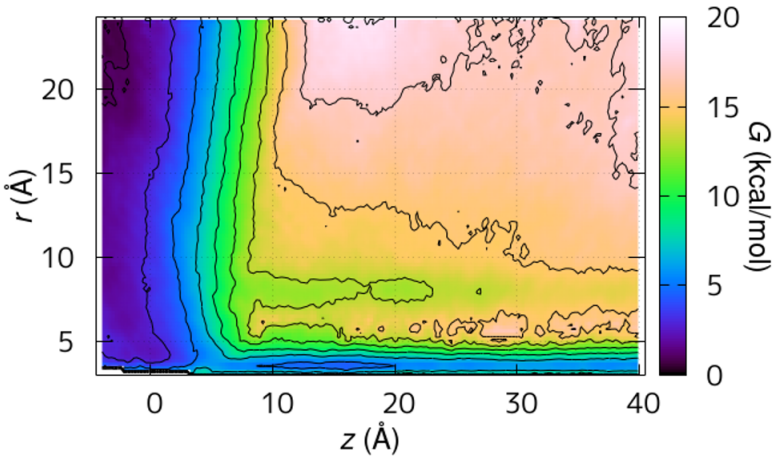

(b)

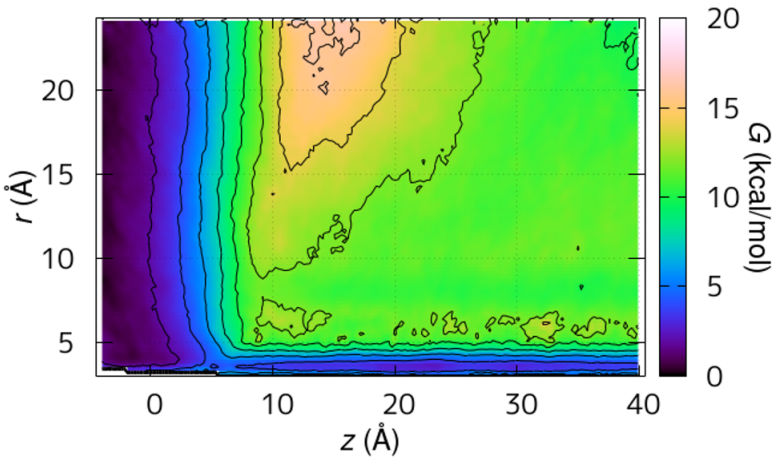

(c)

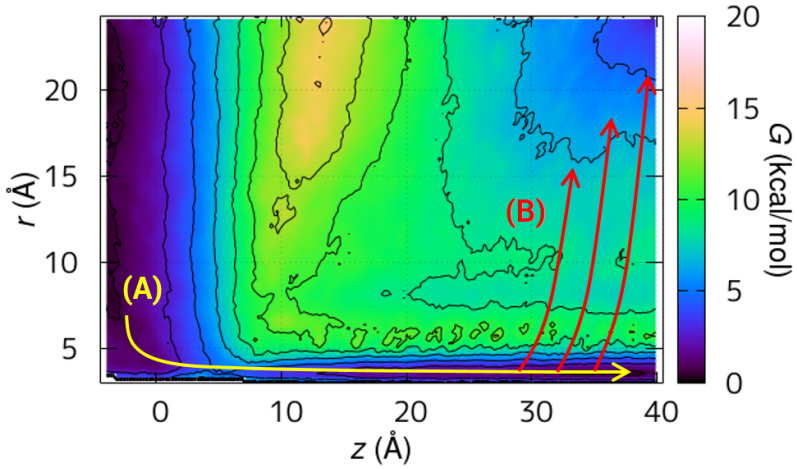

Figure S3: Calculated $G^{(2)}(z, r)$ of F^--THA^+ at water/DCM interface with different values of electric field, (a) $E_z = 0.0$ V/nm, (b) 0.1 V/nm, (c) 0.2 V/nm. The contour lines are drawn with 2 kcal/mol interval. The panel (c) illustrates two exit paths (A) and (B) in yellow and red, respectively.

(a)

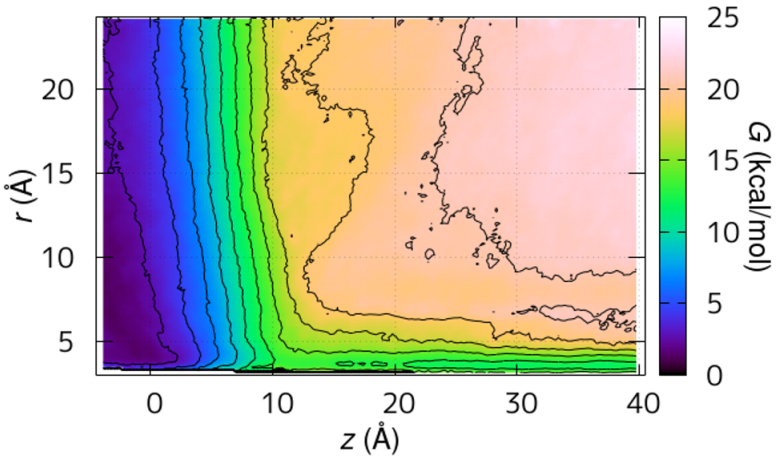

(b)

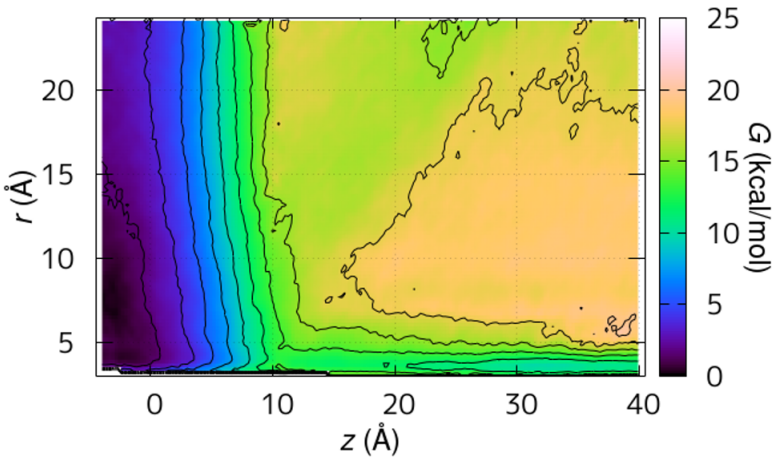

(c)

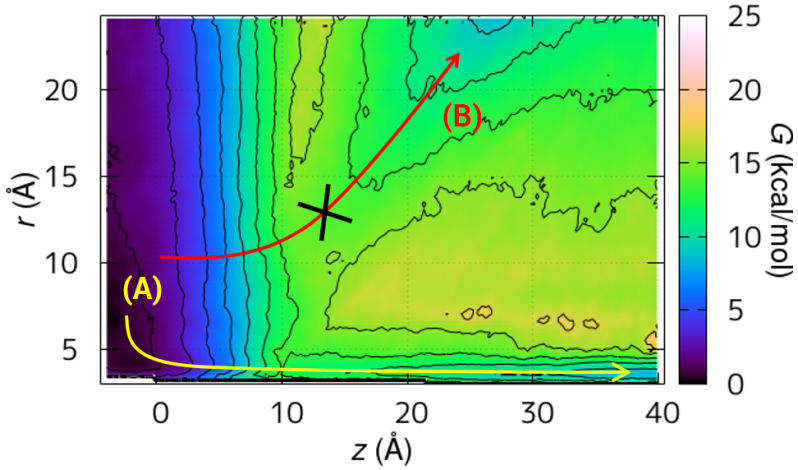

Figure S4: Calculated $G^{(2)}(z, r)$ of F^--TBA^+ at water/DCM interface with different values of electric field, (a) $E_z = 0.0$ V/nm, (b) 0.1 V/nm, (c) 0.2 V/nm. The contour lines are drawn with 2 kcal/mol interval. The panel (c) illustrates two exit paths (A) and (B) in yellow and red, respectively, and $\times$ denotes the transition state of (B).

Å, and reduced the $G^{(2)}(z,r)$ surface to the 1-D profile for the coordinate z by

$$G^{(1),\mathrm{IP}}(z) = -k_B T \ln \int_{0\text{Å}}^{10\text{Å}} 4\pi r^2 dr \exp\left(-\frac{G^{(2)}(z,r)}{k_B T}\right) \tag{S10}$$

We note that the result of $G^{(1),\mathrm{IP}}(z)$ is rather insensitive to the upper bound of the integral, $r = 10$ Å, since the integrated Boltzmann factor in Eq. (S10) is actually dominant in the region of stable ion pair state. The results of free energy profiles for the ion pairs are shown in Figure S5.

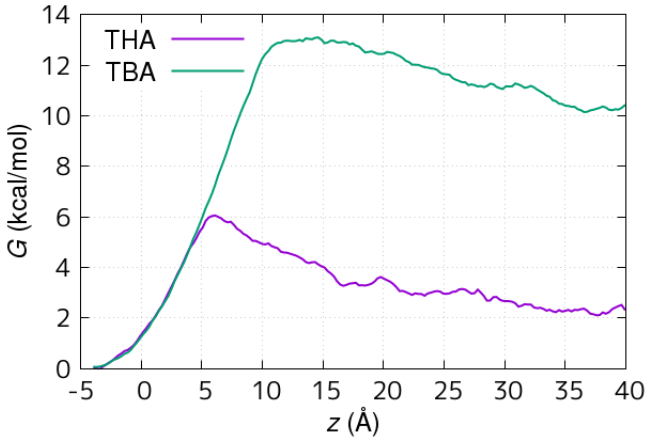

Figure S5: 1-D free energy surface $G^{(1),\mathrm{IP}}(z)$ for the ion pairs, $\mathrm{F}^- - \mathrm{THA}^+$ (purple) and $\mathrm{F}^- - \mathrm{TBA}^+$ (green), in Eq. (S10) under $E_z = 0.2$ V/nm.

The $G^{(1),\mathrm{IP}}(z)$ profiles show that the $\mathrm{F}^- - \mathrm{THA}^+$ and $\mathrm{F}^- - \mathrm{TBA}^+$ ion pairs have asymptotic free energies of about 2 kcal/mol 10 kcal/mol, respectively, under the electric field E_z. The considerable difference in asymptotic free energy by 8 kcal/mol is attributed to the difference in hydrophobicity of THA^+ and TBA^+. The difference will have a significant consequence to determine the transport mechanism, as we discuss later.

S2.3 Radial distribution functions of $\mathrm{THA}^+/\mathrm{TBA}^+$

Before calculating the free energy profiles $G^{(1)}(z)$ for single ions in Sec. S2.4, we need to define the water finger coordinate w for these ions, since $G^{(1)}(z)$ profiles are derived from the calculated results of $G^{(2)}(z,w)$ by Eq. (S6). The water finger coordinate w is given on

the basis of a graph of instantaneous molecular configuration by regarding the ion and water molecules as vertices, and it corresponds to the threshold of edge distance to make the ion reachable to the bulk water.[4,14] To compare the edge distances of water-water and water-ion properly, we need to take account of the difference in molecular size between water and ion. Therefore, we examine the water-ion contact distances in comparison with water-water. The calculated RDFs in bulk water are shown in Figure S6, which includes O–O (purple), F–O (green), N(THA^+)–O (light blue), and N(TBA^+)–O (yellow).

One notices that the N(THA^+)–O and N(TBA^+)–O RDFs do not show conspicuous first solvation peak, in contrast to the O–O or F–O RDFs. Therefore, the contact distance for N–O was evaluated with the difference in the rise distances of N(THA^+/TBA^+)–O and O–O (see the inset of Figure S6). Therefore, the offset value $\Delta R = -1.0$ Å was used for N–O distances to calculate the water finger coordinate w associated to the ions.

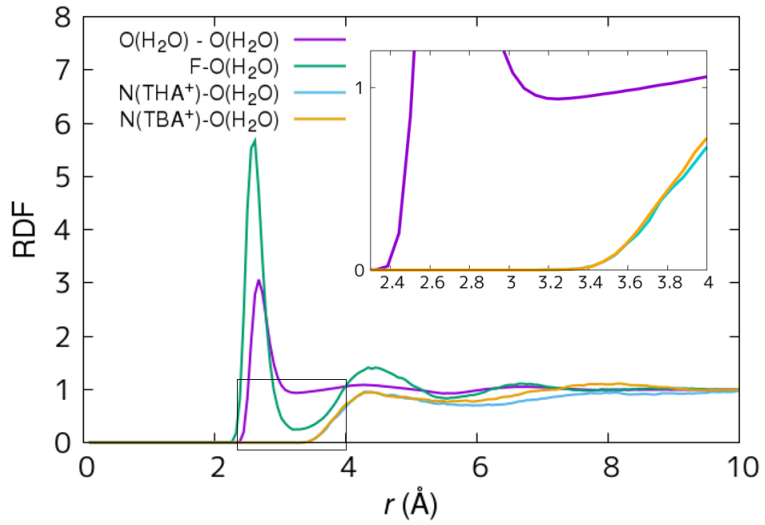

Figure S6: Calculated radial distribution functions: O(H_2O)–O(H_2O) (purple), F–O(H_2O) (green), N(THA^+)–O(H_2O) (light blue), N(TBA^+)–O(H_2O) (yellow) in liquid water. The inset shows a magnified picture for the rise distances.

S2.4 Free energy profiles for single ions

Calculated 1-dimensional free energy profile $G^{(1)}(z)$ of the F^- anion over the water-DCM interface is displayed in Figure S7. The transfer free energy of F^- at no field is calculated to be 18 kcal/mol, which is comparable to the experimental value, 14.0 kcal/mol.[20] Figure S7 shows that the free energy profile of F^- is sensitive to the imposed electric field E_z. With increasing electric field E_z, the asymptotic free energy of the F^- ion decreases in the bulk oil phase ($z \gg 0$) due to the electrostatic force on the negative charge, and accordingly the barrier height of the F^- transfer along the $G^{(1)}(z)$ profile decreases. The present barrier height, 14 kcal/mol, at $E_z = 0.2$ V/nm for the F^- alone is essentially equivalent to the barrier ($\sim$ 14 kcal/mol) at the transition state X for the F^-–TBA^+ system in Figure S4 (c), where TBA^+ forms no transient ion pair during the transport.

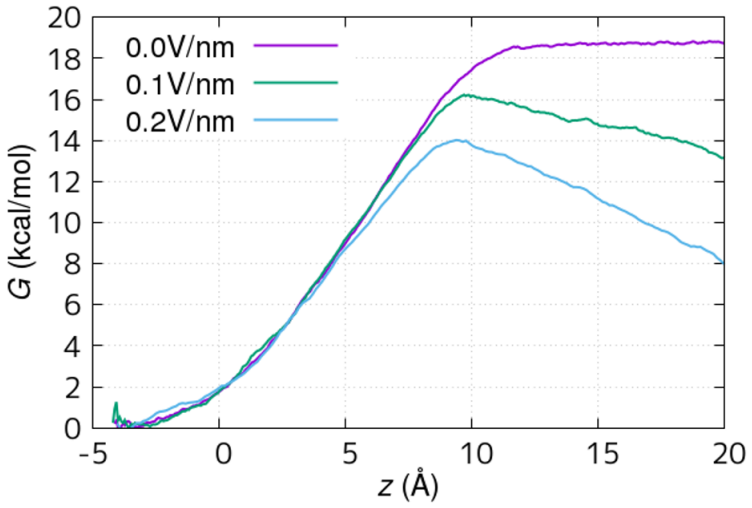

Figure S7: Calculated $G^{(1)}(z)$ profiles of F^- over water-DCM interface. E_z=0.0 (purple), 0.1 (green), 0.2 V/nm (blue).

Figure S8 displays the 1-dimensional free energy $G^{(1)}(z)$ of the cations (THA^+, TBA^+) alone with varying electric field. Under the electric field $E_z = 0.2$ V/nm, both THA^+ and TBA^+ show increasing free energy $G^{(1)}(z)$ with increasing z in the oil phase, which is in contrast to F^- (Figure S7) due to the opposite charge. Under the condition of no field

E_z = 0.0 V/nm, the $G^{(1)}(z)$ profiles of both THA^+ and TBA^+ have minimum near the water-DCM interface $z \approx 2$ Å, indicating slight interface activity of THA^+ and TBA^+.

S2.5 Dissociation of ion pair in oil phase

We also investigate the free energy associated to the formation/break of ion pair in the bulk DCM phase. The break process of the ion pair in the oil phase is involved in the shuttling mechanism of path (B-1). The calculated 1-D free energy surfaces $G^{(1)}(r)$ with respect to the distance between F^- and THA^+/TBA^+ are displayed in Figure S9. The minima of $G^{(1)}(r)$ at $r \approx 3.5$ Å indicates the ion pair, and the free energy barrier for dissociation is evaluated with the maxima of $G^{(1)}(r)$ at $r \approx 6$ Å. We notice that the barrier heights are nearly same between THA^+ and TBA^+ within 1 kcal/mol.

Comparing the panel (a) $E_z = 0.0$ V/mn (no field) with (b) $E_z = 0.2$ V/nm, we notice that the electric field reduces the dissociation barrier by about 1 kcal/mol commonly for both THA^+ and TBA^+ cases. The reduced barrier is readily understood with the electrostatic energy of the ion pair. The electric field E_z tends to align the ion pair along the direction of the field, and consequently the structural change from the ion pair ($r = 3.7$ Å) to the barrier position ($r = 6.0$ Å) accompanies the change in the electrostatic energy of the ion pair. The change in the electrostatic energy under the field $E_z = 0.2$ V/nm is estimated to

$$E_z \cdot \Delta r \simeq 0.2 \text{ V/nm} \times (6.0 - 3.7) \text{ Å} \times 23.06 \text{ kcal/mol/eV} \simeq 1 \text{ kcal/mol} \tag{S11}$$

S3 Discussion – Criteria of Shuttling Mechanism

The essential factor to determine whether the catalytic shuttling mechanism takes place or not is the relative free energy barriers of two possible paths (B-1) shuttling and (B-2) no shuttling. We have argued the relative free energies with Figure 4 of the main text. Here we quantitatively discuss the free energy of each elementary step involved in these paths

(a)

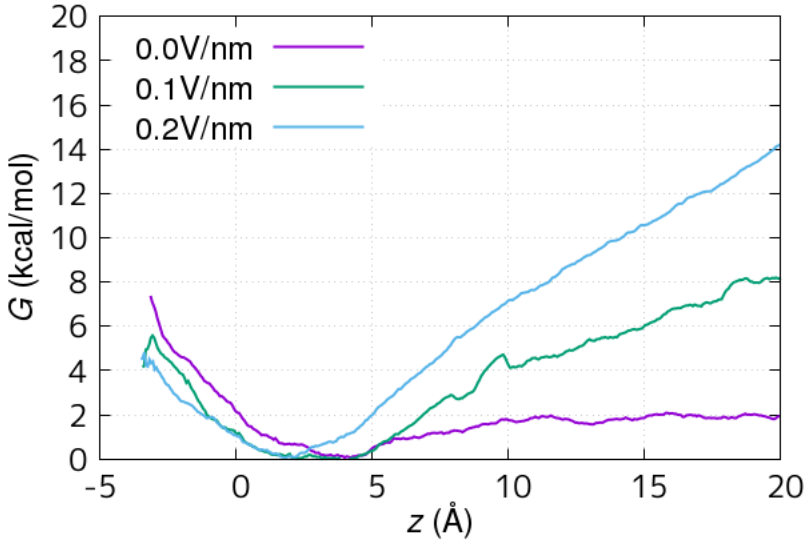

(b)

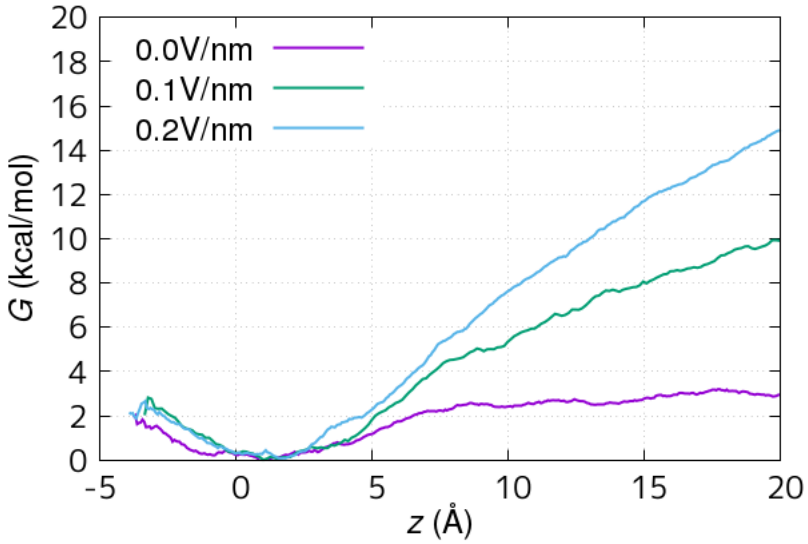

Figure S8: Calculated $G^{(1)}(z)$ profiles over water-DCM interface for (a) THA^+ and (b) TBA^+.

(a)

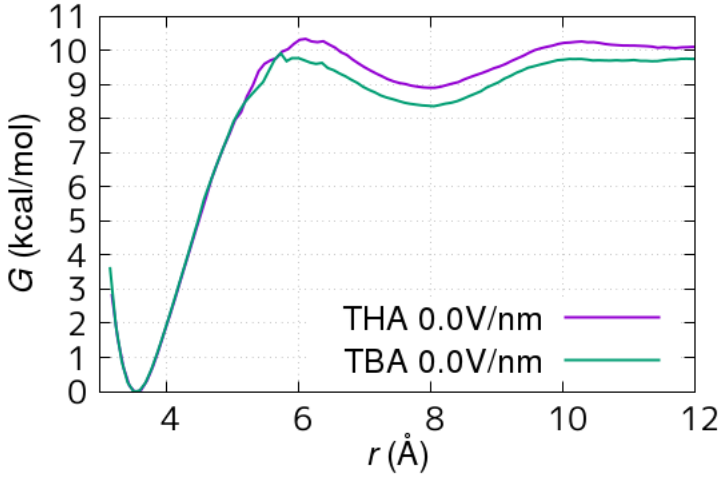

(b)

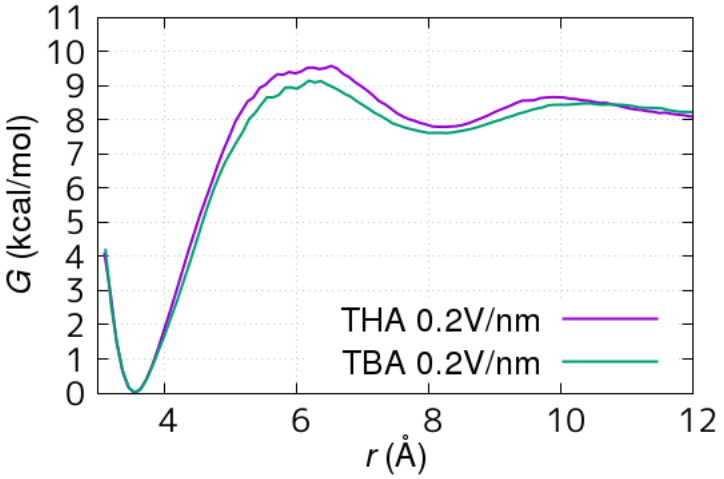

Figure S9: Calculated $G^{(1)}(r)$ as a function of the distance r between F^- and N site of THA^+ (purple) or TBA^+ (green) in the bulk DCM phase. Panel (a) shows the results at no field $E_z = 0.0$ V/nm, and (b) at $E_z = 0.2$ V/nm.

to discuss the net barriers and transport mechanism. In this section we deal with the free energies of F^- transport under the electric field $E_z = 0.2$ V/nm, unless otherwise noted.

The scheme of elementary kinetic steps involved in the two possible paths (B-1) and (B-2) is shown in Figure S10. The (B-1) path is considered as a two-step route; first the ion pair is formed and transported in the oil phase, and then the ion pair breaks to allow the ion to enter the bulk oil phase. On the other hand, (B-2) is a one-step route that the F^- transfers from water to oil phase alone with virtually little role of the ligand.

In the (B-1) path, the first stage of the transport of ion pair over the interface is illustrated in the free energy profile $G^{(1)}(z)$ in Figure S5. The transport of the ion pair has a slight barrier near the interface, and the free energy of transport is estimated to be 2 kcal/mol for F^-–THA^+ and 10 kcal/mol for F^-–TBA^+. The F^-–THA^+ complex is stabler in the oil phase, since THA^+ is more hydrophobic than TBA^+. (Note that the barrier in the first stage is not associated to the rate-determining step, as we show below.) Then the ion pair eventually breaks in the oil phase toward the final state, and this latter stage is illustrated in the free energy profile $G^{(1)}(r)$ in Figure S9. The barrier for dissociation is estimated to be 9.5 kcal/mol for F^-–THA^+ and 9.0 kcal/mol for F^-–TBA^+ from Figure S9 (b). The barrier for the dissociation is found to be nearly unchanged between THA^+ and TBA^+. The net transition state (TS) of the path (B-1) is located in the latter stage to break the transient ion pair.

On the other hand, the (B-2) path involves no transient ion pair, and is equivalent to the transport of F^- alone. The barrier height of (B-2) is essentially equivalent to that of $G^{(1)}(z)$ profile of single F^- in Figure S7, and estimated to be 14 kcal/mol under $E_z = 0.2$ V/nm. In fact, this barrier height ~ 14 kcal/mol agrees with that of the transition state X in Figure S4 (c), where the TS of (B-2) path is well defined in the F^-–TBA^+ case.

Based on the above estimations in Figure S10, we compare the free energies of two possible paths (B-1) and (B-2). The total barrier in the (B-1) path is estimated to be $2 + 9.5 \simeq 11.5$ kcal/mol for F^-–THA^+ and $10 + 9 \simeq 19$ kcal/mol for F^-–TBA^+. On the other hand, the

barrier in the (B-2) path is estimated to be 14 kcal/mol for F^-–THA^+ and F^-–TBA^+, irrespective of the ligand. By comparing the total barrier heights of (B-1) and (B-2), we understand that F^-–THA^+ prefers the (B-1) shuttling path while F^-–TBA^+ prefers the (B-2) no shuttling path. The distinct behavior is mostly attributed to the difference in hydrophobicity of THA^+ and TBA^- which governs the stability of the transient ion pair in the oil phase.

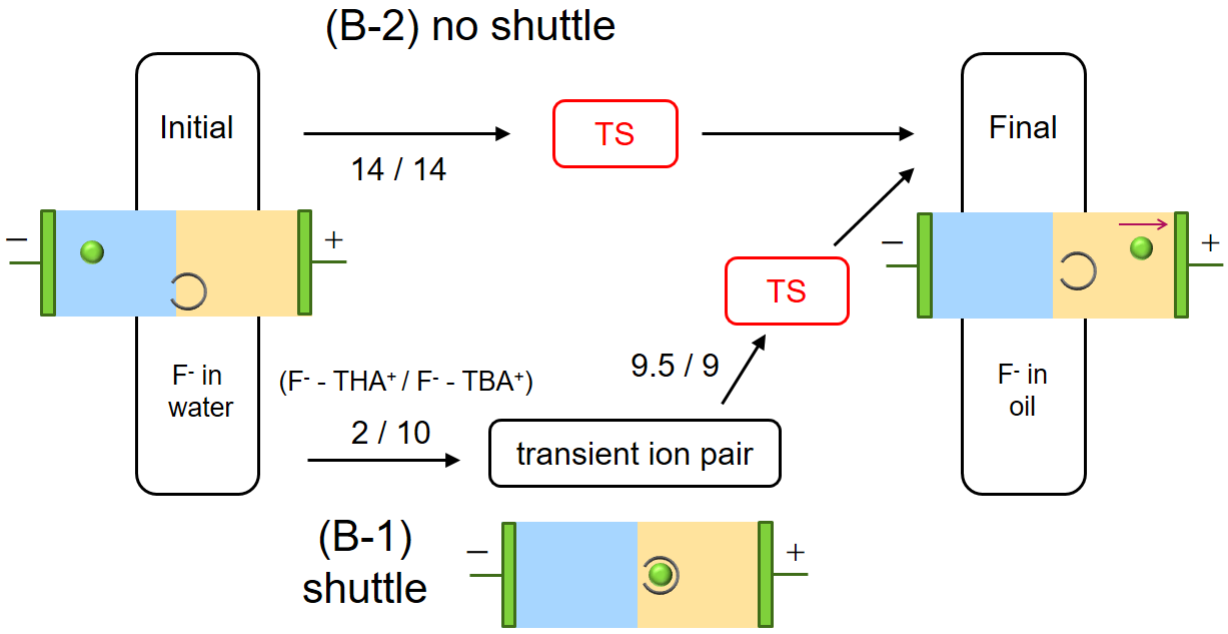

Figure S10: Kinetic scheme of interfacial transport of F^- with THA^+/TBA^+. Two paths (B-1: shuttle) and (B-2: no shuttle) are illustrated with their intermediate and transition states. Two figures associated to an arrow (*e.g.* 2 / 10) mean the estimated free energy costs at each kinetic step for the F^- transfer assisted with THA^+ and TBA^+, respectively, in kcal/mol.

References

(1) Caldwell, J. W.; Kollman, P. A. *J. Phys. Chem.* **1995**, 6208–6219.

(2) Dang, L. X. *J. Chem. Phys.* **1999**, *110*, 10113–10112.

(3) Xantheas, S. S.; Dang, L. X. *J. Phys. Chem.* **1996**, *100*, 3989–3995.

(4) Kikkawa, N.; Wang, L.; Morita, A. *J. Am. Chem. Soc.* **2015**, *137*, 8022–8025.

(5) Dang, L. X. private communication.

(6) Yang, L.; Tan, C.-H.; Hsieh, M.-J.; Wang, J.; Duan, Y.; Cieplak, P.; Caldwell, J.; Kollman, P. A.; Luo, R. *J. Phys. Chem. B* **2006**, *110*, 13166–13176.

(7) Weiner, S. J.; Kollman, P. A.; Case, D. A.; Singh, U. C.; Ghio, C.; Alagona, G.; Profeta, S.; Weiner, P. *J. Am. Chem. Soc.* **1984**, *106*, 765–784.

(8) Weiner, S. J.; Kollman, P. A.; Nguyen, D. T.; Case, D. A. *J. Comp. Chem.* **1986**, *7*, 230–252.

(9) Darden, T.; York, D.; Pedersen, L. *J. Chem. Phys.* **1993**, *98*, 10089–10092.

(10) Toukmaji, A.; Sagui, C.; Board, J.; Darden, T. *J. Chem. Phys.* **2000**, *113*, 10913–10927.

(11) Darvas, M.; Jourge, M.; Cordeiro, M.; Jedlovsky, P. *Journal of Molecular Liquids* **2014**, *189*, 39–43.

(12) Sugita, Y.; Kitao, A.; Okamoto, Y. *J. Chem. Phys.* **2000**, *113*, 6042–6051.

(13) Kumar, S.; Rosenberg, J. M.; Bouzida, D.; Swendsen, R. H.; Kollman, P. A. *J. Comp. Chem.* **1992**, *13*, 1011–1021.

(14) Kikkawa, N.; Wang, L.; Morita, A. *J. Chem. Phys.* **2016**, *145*, 014702.

(15) Nosè, S. *J. Chem. Phys.* **1984**, *81*, 511–519.

(16) Hoover, W. G. *Phys. Rev. A* **1985**, *31*, 1695–1697.

(17) Frenkel, D.; Sumit, B. *Understanding Molecular Simulation*, 2nd ed.; Academic Press: San Diego, 2002.

(18) Andersen, H. C. *J. Comp. Phys.* **1984**, *52*, 24–34.

(19) Allen, M. P.; Tildeslay, D. J. *Computer Simulation of Liquids*; Oxford University Press: Oxford, 1987.

(20) Sabela, A.; Mareček, V.; Samec, Z.; Fuoco, R. *Electrochim. Acta* **1992**, *37*, 231–235.